

UNIVERSITÀ DEGLI STUDI DI PADOVA

Dipartimento di Fisica e Astronomia “Galileo Galilei”

Corso di Laurea in Fisica

Final dissertation

Characterization of the final readout electronics for the large PMTs of the JUNO experiment

Thesis supervisor

Prof. Alberto Garfagnini

Candidate

Vanessa Cerrone

Thesis co-supervisor

Dr. Katharina von Sturm

Academic Year 2020/2021

Abstract

The Jiangmen Underground Neutrino Observatory (JUNO) is a multi-purpose neutrino experiment under construction in South China. It's a 20 kton liquid scintillator (LS) detector contained in a spherical acrylic vessel with an inner diameter of 35.4 m. The light emitted by the LS is watched by 17612 20-inch PMTs and 25600 3-inch PMTs. An unprecedented energy resolution and a large fiducial volume offer an extensive neutrino and astroparticle physics program.

The JUNO Padova research group is responsible for the design and development of the large PMT readout electronics. The PMT output signal is amplified and converted to digital with a 14 bit, 1 GS/s Analog-to-Digital-Converter (ADC). The signal is further processed (local trigger generation, charge reconstruction and timestamp tagging) and stored temporarily in a local memory before being sent to the data acquisition (DAQ), once validated by the global trigger electronics. To verify the performances of the electronics, a small experiment with 48 small size PMTs reading out the light coming from a 20 liter liquid scintillator detector has been assembled and setup at the Legnaro INFN National Laboratories (LNL). The setup is equipped with external LED and laser systems, plastic scintillators for cosmic muons trigger and several low-activity gamma sources for calibrating the reconstructed energy.

Within this context, during my thesis work, the performances of the full electronics chain have been investigated in terms of two of its main aspects: linearity of the ADC and time reconstruction. The first part of the work aims at verifying the linearity response of the electronics. Tests are carried out using laser pulses as signal source and a complete calibration of the electronics is performed in terms of energy (charge) reconstruction. Furthermore, the timing correlation properties between different acquisition channels are evaluated; these studies allow to verify the trigger synchronization accuracy expected by the specifics of the large PMTs electronics and required by the experiment. Finally, similar analyses to evaluate the electronics performance and quality are conducted using a different experimental setup equipped with a large (20-inch) PMT.

Contents

1	Introduction	1
1.1	The JUNO Experiment	1
1.2	JUNO experimental apparatus overview	2
1.2.1	JUNO electronics readout	2
2	The integration test facility at LNL	4
2.1	Experimental setup	4
2.2	The electronics chain of the Legnaro test facility	5
3	Laser linearity measurements	7
3.1	Laser calibration with Power Meter	7
3.1.1	Stability analysis	7
3.1.2	Calibration fit	7
3.2	Data acquisition	8
3.2.1	Laser measurements with High Gain ADC	10
3.2.2	Laser measurements with Low Gain ADC	12
3.2.3	Comparison between LG and HG	12
4	Timing analysis	14
4.1	Trigger and timing system	14
4.2	Study of time correlated signals	14
4.3	Trigger time stability	16
5	Measurements with large PMT	18
5.1	Experimental setup	18
5.1.1	Acquired data	18
5.2	Linearity analysis	19
6	Conclusions and future perspectives	20
Appendices		21
A	Detailed results of laser linearity measurements	21
B	Detailed results of timing analysis	24
References		27

Introduction

1.1 The JUNO Experiment

The Jiangmen Underground Neutrino Observatory (JUNO) [1, 2] is a next-generation neutrino experiment under construction in South China, expected to begin data taking in 2023, whose aim is to tackle unresolved issues of neutrino physics and astrophysics. The experiment has been proposed with the main goals of determining the neutrino mass ordering (NMO) at 3σ significance in 6 years and provide a measurement of three oscillation parameters with subpercent precision. Moreover, JUNO will be able to detect supernovae burst neutrinos, solar neutrinos, atmospheric neutrinos and geoneutrinos [3].

The experiment is located under the Dashi hill, 43 km southwest of Kaiping city, next to Jianmeng city. A map of the region is provided in **Figure 1.1**. The site location is optimized to have the best sensitivity for the mass hierarchy determination, which is at 53 km from both the Yangjiang and Taishan Nuclear Power Plants (NPPs), where six and four nuclear cores are planned, respectively. Additionally, a reference detector will be installed at a few meters from the Thainshan reactor core: the Thainshan Antineutrino Observatory (TAO) [4] is a liquid scintillator detector designed to achieve precise measurements of the reactor antineutrinos spectrum, so it has a key role in the NMO determination.



Figure 1.1 – Location of the JUNO site. The distances to the nearby Yangjiang and Taishan Nuclear Power Plants (NPPs) are both 53 km. Daya Bay NPP is 215 km away. Three metropolises, Hong Kong, Shenzhen, and Guangzhou, are also shown.

1.2 JUNO experimental apparatus overview

The JUNO detector consists of a Central Detector (CD), a water Cherenkov detector and a Top Tracker (TT). A schematic view of the JUNO detector is shown in **Figure 1.2** [3]. The CD is a liquid scintillator (LS) detector with a designed effective energy resolution of $\sigma_E/E = 3\%/\sqrt{E(\text{MeV})}$. It contains 20 kton LS in a spherical acrylic vessel, which is submerged in a water pool, that has a diameter of 43.5 m and a height of 44 m, providing sufficient buffer in all directions to protect the LS from the surrounding rock radioactivity. The acrylic vessel is supported by a stainless steel (SS) structure via Connecting Bars. The light emitted by the LS is watched by 17612 20-inch PMTs (“Large PMTs”) and 25600 3-inch PMTs (“Small PMTs”), which are installed on the inner surface of the SS Main Structure. The water pool is equipped with PMTs to detect the Cherenkov light from cosmic muons, acting as a veto detector. Compensation coils are mounted on the SS structure to suppress the Earth’s magnetic field and minimize its impact on the photoelectron collection efficiency of the PMTs. The CD and the water Cherenkov detector are optically separated. On top of the water pool, there is a plastic scintillator array, i.e. Top Tracker, to accurately measure the muon tracks. A chimney for calibration operations connects the CD to the outside from the top. The calibration systems are operated in the Calibration House, above which a special radioactivity shielding and a muon detector are designed.

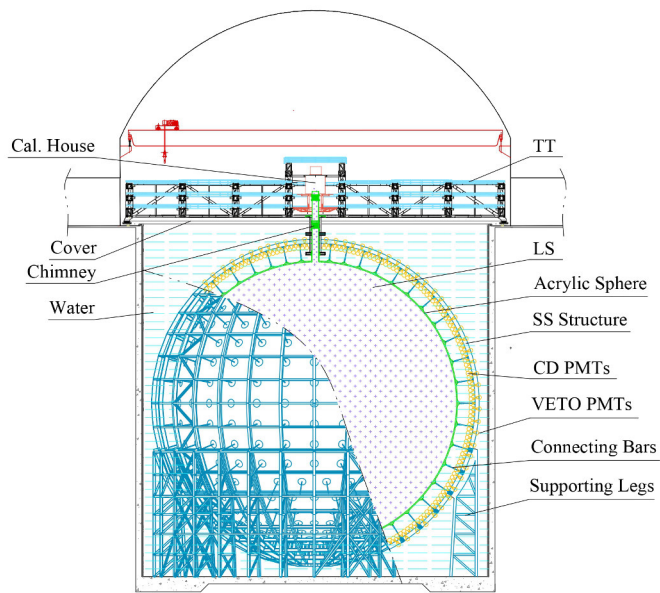


Figure 1.2 – Schematic view of the JUNO detector

1.2.1 JUNO electronics readout

The ambitious goal of the JUNO detector, to determine the NMO, requires an excellent energy resolution of 3% at 1 MeV. From the perspective of PMTs, the key ingredients to reaching this energy resolution are a large photodetector area coverage, high photon detection efficiency, low dark noise, and stable operation of the whole PMT system. The average number of photoelectrons (PE) generated by a single large PMT ranges from one PE for low-energy events up to thousands PE. In both cases, the photoelectrons’ time profiles have to be determined and the energy of the event has to be measured. A basic limitation on the energy resolution arises from the statistics of detected PE and it must not be worsened significantly by the effect of electronics. Hence, the design of the large PMT

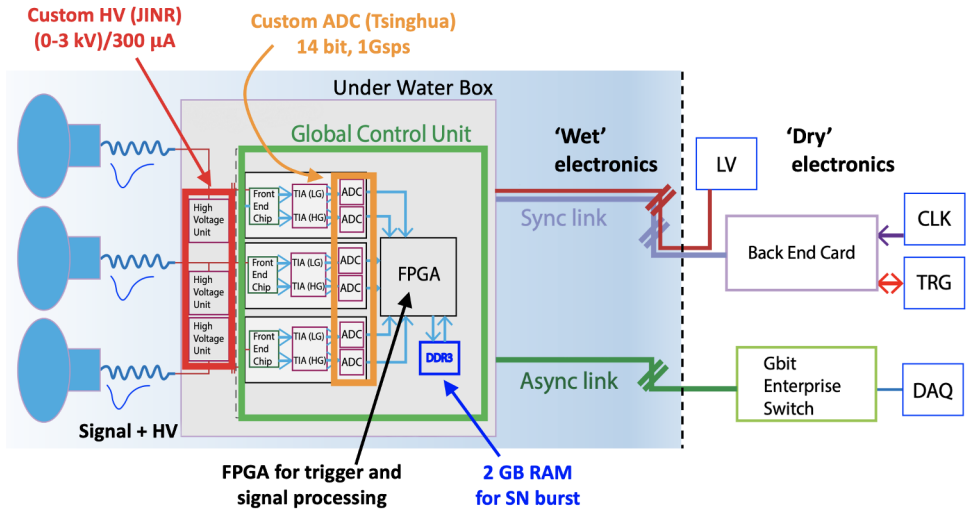


Figure 1.3 – Large PMT electronics scheme: the “wet” electronics (left) is connected to the “dry” electronics by means of Ethernet cables and a dedicated low impedance cable for power distribution.

electronics [5] has been driven by these requirements.

The layout of the large PMT electronics is reported in **Figure 1.3**. The large PMT electronics is split into two parts: the “wet” electronics, located a few meters from the PMTs inside a custom stainless steel box (UWbox), and the “dry” electronics in the electronics rooms. The “wet” electronics is made of the following components:

- Base: PMT voltage divider and splitter. Three PMT output signals are fed to the front-end and readout electronics located inside the UWbox;
- High Voltage Unit (HVU): a custom module that provides the bias voltage to the voltage divider;
- Global Control Unit (GCU): it receives the analog signal, which is amplified and converted to digital with a 14 bit, 1 GS/s, custom ADC. The signal is further processed (local trigger generation, charge reconstruction and timestamp tagging) and stored temporarily in a local memory before being sent to the data acquisition (DAQ), once validated by the global trigger electronics. Besides the local memory available in the readout-board FPGA¹, a 2 GBytes DDR3 memory is available and used to provide a larger memory buffer in the exceptional case of a sudden increase of the input rate;
- the readout electronics is connected to the “dry” electronics through the so-called “synchronous link”, which provides the synchronous Clock (CLK) and Trigger (TRG) links, and an “asynchronous link” which is dedicated to the DAQ.

The “dry” electronics is composed of the Back End Card (BEC) which receives and sends the digital data, distributes the power, and handles the synchronous signals (CLK and TRG), the trigger electronics, the central JUNO clock synchronized to GPS and the power supplies. The large PMT electronics can work with a centralized “global trigger” mode, where the information from the single PMTs is collected and processed in a Central Trigger Unit (CTU). The latter validates the trigger based on a simple PMT multiplicity condition or a more refined one. Upon a trigger request, validated waveforms are sent to the DAQ event builder through the Gigabit Ethernet asynchronous link.

¹Field Programmable Gate Array (FPGA) which is an Integrated Circuit designed to be configured by a customer or a designer after manufacturing (hence field-programmable).

The integration test facility at LNL

The Front-End electronics of the experiment is required to be extremely reliable, due to the fact that it will be put into sealed boxes at a maximum water depth of 40 m, making it impossible to access it after its installation. The tolerance requirement for the PMTs is less than 0.5 % defective channels over 6 years of operational time [3]. In addition to that, the optimization of the whole electronics chain is crucial: for this purpose an integration test facility that allows to have a characterization of the system response and to test the JUNO electronics performances has been developed. In order to test the electronics, a small JUNO mock-up system has been built at the Laboratori Nazionali di Legnaro (LNL), in Italy.

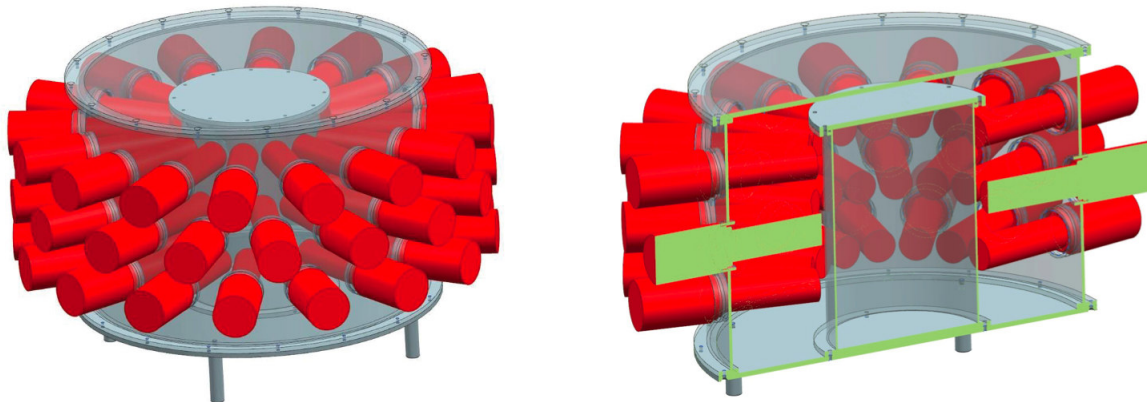


Figure 2.1 – Mechanical design of the test facility; the internal cylindrical vessel (grey) is surrounded by the 48 PMTs (red); the PMTs are inside the plastic structure (grey), while their bases are outside.

2.1 Experimental setup

This test facility, shown in **Figure 2.1**, recreates the Central Detector structure and is composed by:

- an internal cylindrical vessel, made of transparent Plexiglas, containing about 17 l of liquid scintillator made by a solvent (LAB) doped with Poly-Phenylene Oxide (PPO) and p-bis-(o-MethylStyryl)-Benzene (bisMSB), used as wavelength shifter to match the PMT response. The same recipe of JUNO LS is used [6];
- the internal cylinder is surrounded by 48 Philips XP2020 PMTs with a diameter of $\simeq 5$ cm. As it's shown in **Figure 2.1**, the PMTs are placed towards the inside, all around the cylindrical vessel, and they are divided into three rings, each of 16 PMTs. They are connected, in groups of three, to 16 Global Control Units (GCUs), which have 3 channels (labeled 0,1,2) each. These

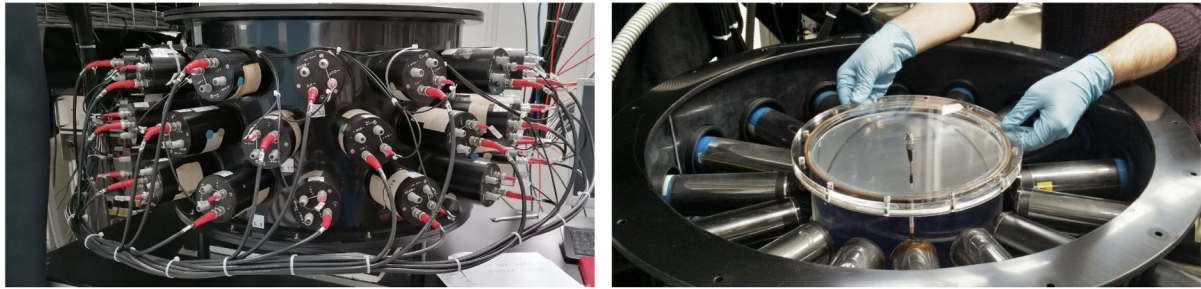


Figure 2.2 – Picture of the test facility at LNL: the black plastic structure and the PMTs (on the left), the liquid scintillator vessel and the PMTs bases (on the right) are visible.

photomultiplier tubes feature a high cathode sensitivity, good linearity, a very low background noise, good single electron spectrum and they are suitable in experiments where the number of photons to be detected is very low [7]. During the data analysis it might be crucial to determine whether or not the PMTs placed in the various rings collect a comparable amount of charge, due to their different position with respect to the source;

- a black plastic structure, which can be seen in **Figure 2.2**, surrounds the inner vessel. It's used to support the PMTs and to shield the liquid scintillator vessel from external light. For the same purpose, a black cloth covers the whole structure;
- 3 plastic scintillators, one placed on the top of the apparatus and the other two under the black plastic structure, aim at detecting muons coming from cosmic rays. They are used to provide a trigger mechanism if the AND coincidence of these three scintillators is satisfied;
- a laser light source has been introduced using an optical fiber and a diffuser inside the liquid scintillator vessel: it provides fast pulses and it's used to determine a calibration and characterization of the electronics.

2.2 The electronics chain of the Legnaro test facility

The electric signal obtained from the collected charge by the PMTs has to pass through several steps of the electronics chain, before being stored in the raw data files produced by the Data Acquisition (DAQ) program.

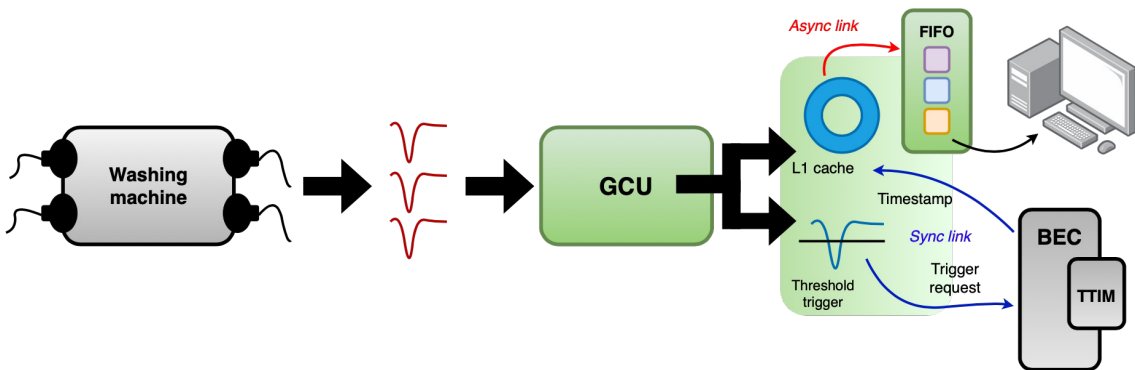


Figure 2.3 – Scheme of the electronics chain of the Legnaro test system.

As previously anticipated, the 48 PMTs are connected, in groups of 3, to 16 GCUs; nevertheless, only 13 GCUs, thus 39 available acquisition channels, are currently active. The electronics chain, whose

schematic description is reported in **Figure 2.3**, works accordingly to the following steps:

- the channels acquire their signals concurrently;
- for each active GCU channel, the analog signal produced by the PMT is digitized by an Analog-to-Digital Unit (ADU) and subsequently doubled: one of the two signal copies is registered with its GCU timestamp into a L1 cache, while the other one is analyzed with a specific threshold trigger algorithm. The ADU has a custom current preamplifier with 2 ranges, low gain (8:1, 0 - 1000 PE) and high gain (1:1, 0 - 128 PE), and a custom design high-speed ADC, with 14-bit resolution and 1 GS/s sampling time;
- if the signal exceeds a fixed threshold, the GCU sends a trigger request to a Back End Card (BEC) which is responsible for the communication between 48 GCUs, the Data Acquisition system (DAQ), the power and the timing and trigger distribution system (the latter through the Trigger and Timing (TTIM) FPGA Mezzanine Card). The TTIM then takes a “global trigger” decision, based on the chosen trigger logic, and it sends back to all the GCUs the same timestamp, chosen by the trigger validation; for this step, GCUs and BEC must be properly synchronized in time [8]. In particular, the global trigger logic could be based either on a logic OR of all the 3 channels of a single GCU, or on the multiplicity of the acquired event, i.e. a logic AND between two or more channels. In addition to this trigger validation procedure, the system implements an additional external trigger that can be used, for instance, to trigger on different types of events;
- after the trigger validation by the BEC, the firmware retrieves the signals with the selected timestamp from the L1 cache and it ports them into a First-In-First-Out (FIFO) unit; the content of the FIFO is then transferred to the DAQ server through an ethernet switch, where the DAQ program stores the raw data accordingly to a fixed structure.

Laser linearity measurements

The main part of the thesis is focused on providing a precise characterization of the electronics and on verifying its linearity response. For this purpose, a pulsed laser source, characterized by a known wavelength, has been employed to perform a precise calibration procedure.

3.1 Laser calibration with Power Meter

We used the Hamamatsu PLP-10 ultrashort pulsed light source, which consists of an M10306 laser diode head and a C10196 controller [9]. It provides fast pulses with a FWHM of around 52 ps at a wavelength of 403 nm. The controller allows to change the emission frequency from 1 Hz to 100 MHz, and the laser intensity can be adjusted either by operating on a potentiometer that has a range that goes from 5 to 15 a.u. (*arbitrary units*) or by means of external optical filters. Using a Thorlabs PM16-140 compact USB Power Meter [10] with an integrating sphere sensor, it was possible to monitor in real-time the power output in microwatts, in order to find the right conversion from arbitrary units to SI units. Therefore, a calibration fit has been performed, studying the functional relation between the values acquired by the Power Meter and the intensity set on the controller.



Figure 3.1 – Laser head and optical fiber.

3.1.1 Stability analysis

Firstly, a series of samples at different intensities (i.e. 6, 10 and 14 a.u.) were digitized at regular time intervals so as to monitor laser stability during time. As it can be noticed in **Figure 3.2**, the laser output turns out to be stable enough, showing just a slight increase over time, which could be correlated with ambient temperature. Another crucial point was to verify repeatability: a few samples at fixed intensity were acquired, each time switching off the laser. Although intensity fluctuations between the various acquisitions were negligible, laser emission takes a few seconds to stabilize, mostly in the lower power range, as it is evident in **Figure 3.3b**.

3.1.2 Calibration fit

The next step is to experimentally obtain a conversion of the emitted power value set on the controller to SI units. For this purpose, as already anticipated, a Power meter has been used: once the intensity on the controller has been fixed, it allows to read on a computer the corresponding value in SI units. In **Figure 3.3a** it's possible to highlight two main aspects: firstly, the laser is not characterized by a linear response and secondly it shows a different trend according to the intensity range which is taken

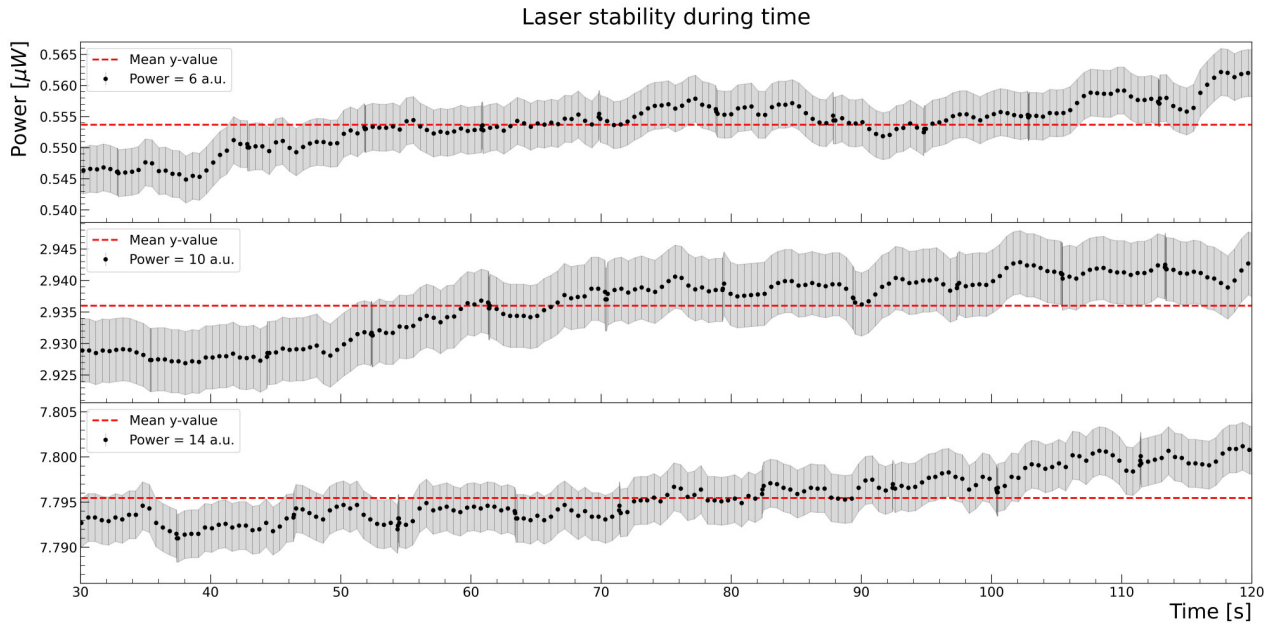


Figure 3.2 – Time distribution of acquired data with Power Meter

into consideration; this behaviour is likely to be imputed to its intrinsic specifics.

Therefore, in order to have accurate calibration parameters, we chose to perform separated polynomial regressions for the two output intensity ranges. The uncertainties associated to the y-values in **Figure 3.3a** (i.e. data acquired with the Power Meter) were calculated by adding in quadrature the random (0.001 μW resolution) and systematic components (1% linearity [10]). In **Figure 3.3a** fit results and residuals are reported.

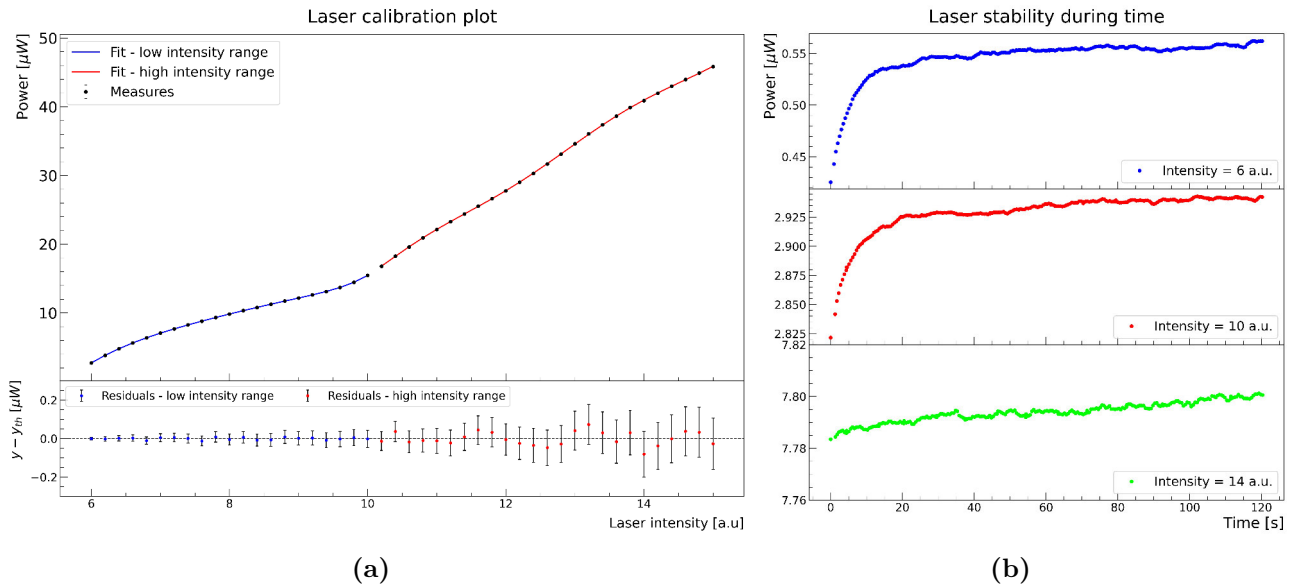


Figure 3.3 – (a) Laser calibration fit with residuals. (b) Example of acquired data with Power Meter to study laser stability.

3.2 Data acquisition

In this section, we will present a description of the acquired data and of the procedure to extract information on the energy deposited by particles in the liquid scintillator (LS), in order to verify the

linear response of the electronics. The processing software stores the data in a ROOT TTree object, written in an output ROOT file, which is composed of different branches that contain information regarding:

- GCU and channel numbers;
- waveform related characteristics (baseline, baseline sigma, minimum, maximum);
- timing (timestamp, trigger number, trigger time);
- data quality (e.g. threshold flag, errors, valid data);
- integrated charge (single PMT or total charge).

In particular, the collected charge is reconstructed by calculating the integral of the signal waveform within a fixed time interval, which has to be carefully evaluated according to the specific acquisition. The charge collected by the single PMT is calculated considering that 1 ADC count equals to 75 μ V (600 μ V for the Low Gain ADC) and taking into account the expected output impedance of 50 Ω seen by the PMTs. In addition to that, the total charge branch in the TTree is used to store the value of the total integrated charge, calculated by summing the charge values extracted from each active channel. In **Figure 3.4** a typical reconstructed signal of one channel, corresponding to a single event, is reported:

- the baseline is calculated as the mean value of a variable number of bins in the pre-trigger region (red box in **Figure 3.4**), i.e. the time window (in ns) in which the signal is yet to exceed the threshold level, which can be adjusted during acquisition;
- the waveform is subtracted from the baseline and then the charge is calculated as the integral of the current in a given time window (highlighted in blue in **Figure 3.4**).

Both baseline and signal time windows are fixed for all events in an acquisition run. For each PMT a distribution, as the one shown in **Figure 3.5** is produced.

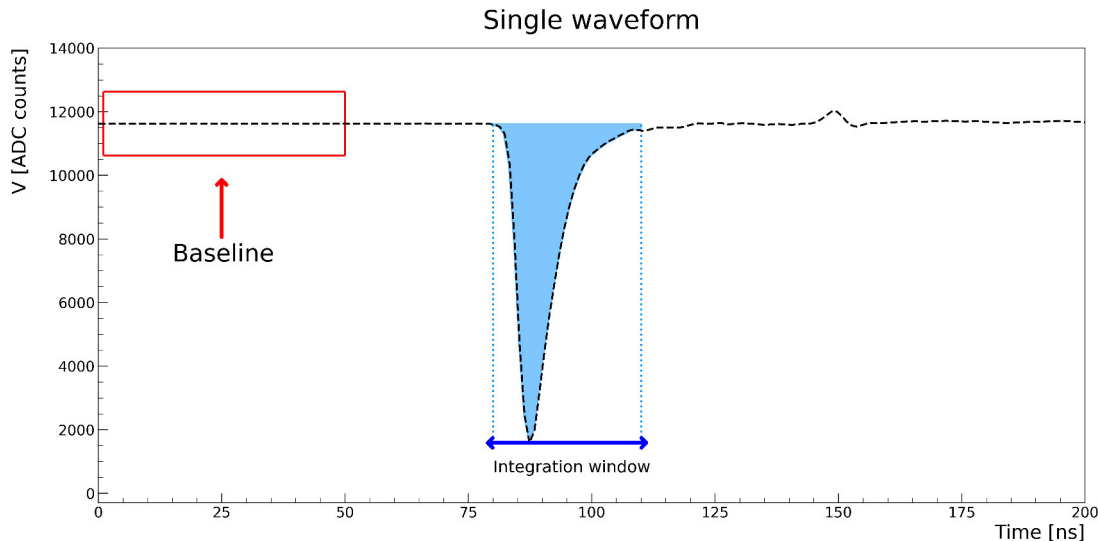


Figure 3.4 – Example of acquired waveform for laser photons interacting in the LS, with the pre-trigger region used in the baseline calculation (in red) and integration time window (in blue). In this case 1 ADC count corresponds to 75 μ V.

After some data quality monitoring, aimed at establishing the proper pre-trigger and time windows, we performed several 60 seconds-long acquisitions varying laser power and using the two ADCs with

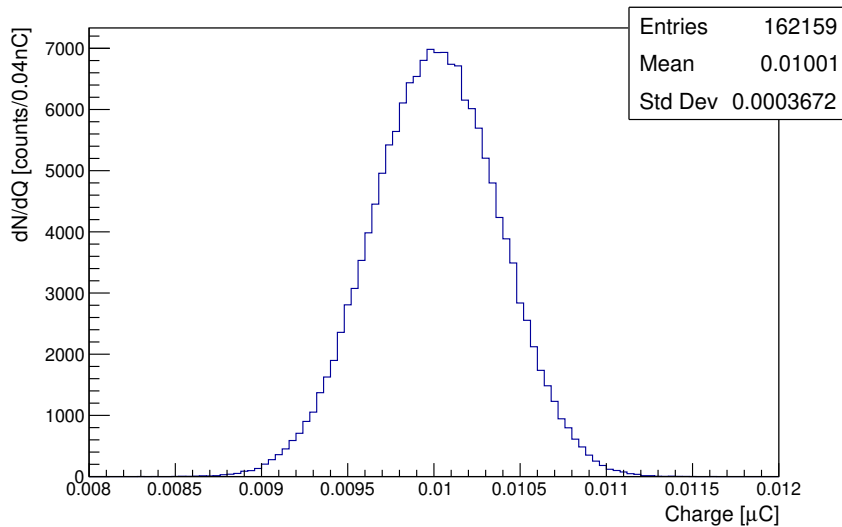


Figure 3.5 – Example of charge spectrum obtained for a single PMT with laser measurements.

different dynamic ranges, in order to study saturation conditions. During this thesis work GCU0 channel 0 and GCU1 channel 2 were not available, so data from 37 channels is analyzed. The trigger output provided by the laser pulse was used as an external trigger; since it is too short (few ns) to be used as an external trigger to the BEC, it's necessary to employ an external pulse generator (HP 8116A) to modify the duration of the trigger signal. A schematic description of the connections is provided in **Figure 3.6**. The following parameters were set on the generator:

- amplitude : HIGH = 5 V, LOW = 0 V;
- width: 100 ns;
- trigger mode and rising edge.

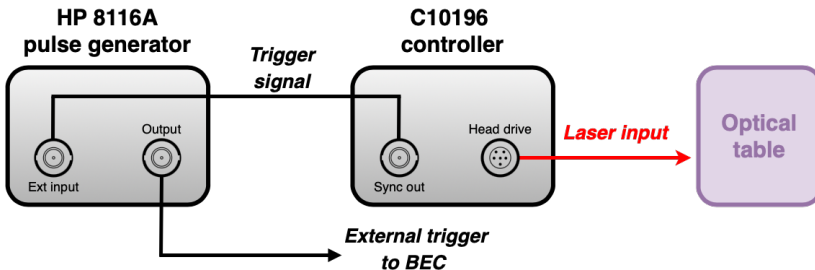


Figure 3.6 – Schematic description of the connections.

The emission laser rate was always set at 1 kHz, unless otherwise specified. Additionally, in order to reduce the optical power of the incident beam, absorptive neutral density filters have been implemented; in particular, Thorlabs NE10B and NE20B filters, which attenuate the beam to 10 % and 1% of the incident power respectively, have been employed.

3.2.1 Laser measurements with High Gain ADC

In this section, results obtained using the High Gain (HG) ADC are presented. As described in the previous section, data from all 37 channels has been acquired varying laser output power from 6.0 to 9.4 a.u. in steps of 0.2. The aim of this analysis is to verify under which circumstances the electronics

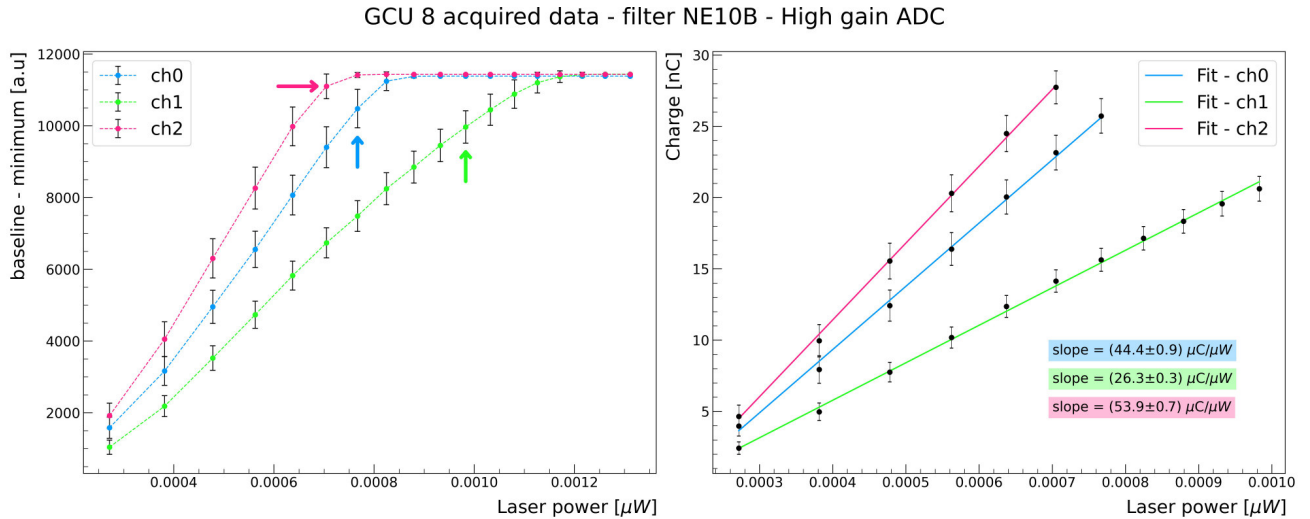


Figure 3.7 – Example of acquired data (GCU8): signal amplitude (on the left) and collected charge (on the right) in function of laser emitted power. Arrows define the linearity range that is consequently considered in the linear regression.

has the expected linear response. First of all, information about the charge collected by the single PMTs is retrieved from the specific TBranch, then the centroids and sigmas of the histograms (see **Figure 3.5**) are extracted. In **Figure 3.7** an example of the results is shown: on the left side the amplitude of the signal (i.e. baseline - minimum) in a.u., acquired by the three channels of GCU8, are reported in function of laser power in SI units calculated using the calibration parameters obtained in **Section 3.1.2**; we can notice that the response is linear up to saturation conditions, which are easily observable on the left plot. The average collected charge is plotted against the input power on the right panel of **Figure 3.7** and a linear regression is performed. The plot shows good linearity and the maximal deviation from a linear fit is $\simeq 6.5\%$.

The same analysis and fit procedure were carried out for all GCUs and results are provided in **Figure 3.8**. The latter shows the slope values returned by the regression in function of a specific ID which univocally identifies GCU and channel numbers. Looking at **Figure 3.8** from left to right, a slightly decreasing trend can be highlighted. For instance, the photomultiplier tubes located in the low ring (black data points in **Figure 3.8**) output an overall amount of charge larger than the other PMTs. This behaviour might indicate a non-uniform photoelectron collection by the PMTs, which is further investigated in the following sections.

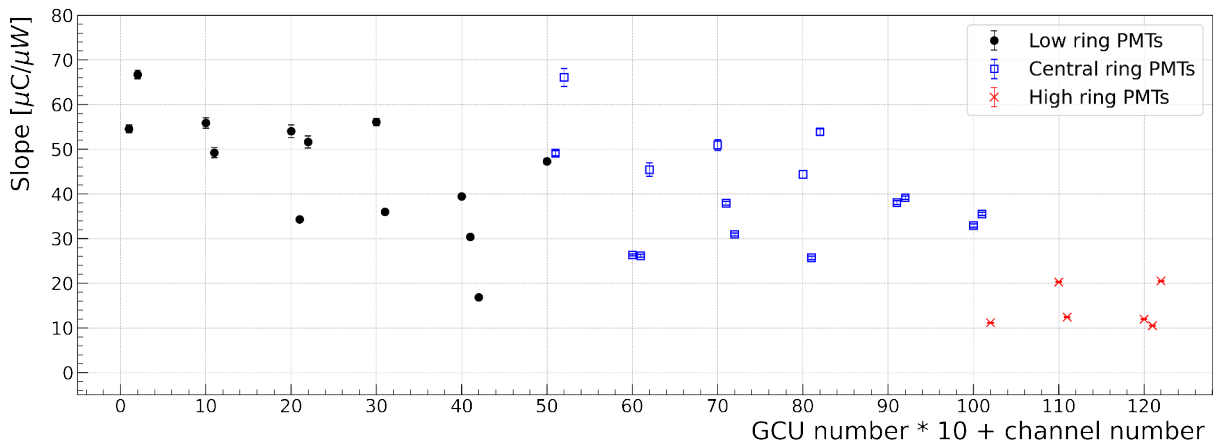


Figure 3.8 – Slope distribution in function of channel ID. Data points are divided according to the PMTs position inside the vessel.

3.2.2 Laser measurements with Low Gain ADC

In this section, results obtained using the Low Gain (LG) ADC are presented. Data from all 37 channels has been acquired varying laser output power from 6.0 to 15 a.u. in steps of 0.5. In **Figure 3.9** an example of the results is shown: the mean collected charge by the three channels of GCU7 and the signal amplitude (i.e. baseline - minimum) in a.u. are reported in function of laser power in SI units. Due to its wider dynamic range with respect to the High Gain ADC, saturations conditions are not reached. The collected charge and the signal amplitude show a good linear trend for high power values, whereas deviations are not negligible in the lower power range. This result emphasizes the importance of efficiently exploiting the dynamic range of the ADC, in order to have an adequate signal-to-noise ratio; indeed, the LG ADC is not suitable to resolve very small signals, which may not be distinguishable from the electronics noise.

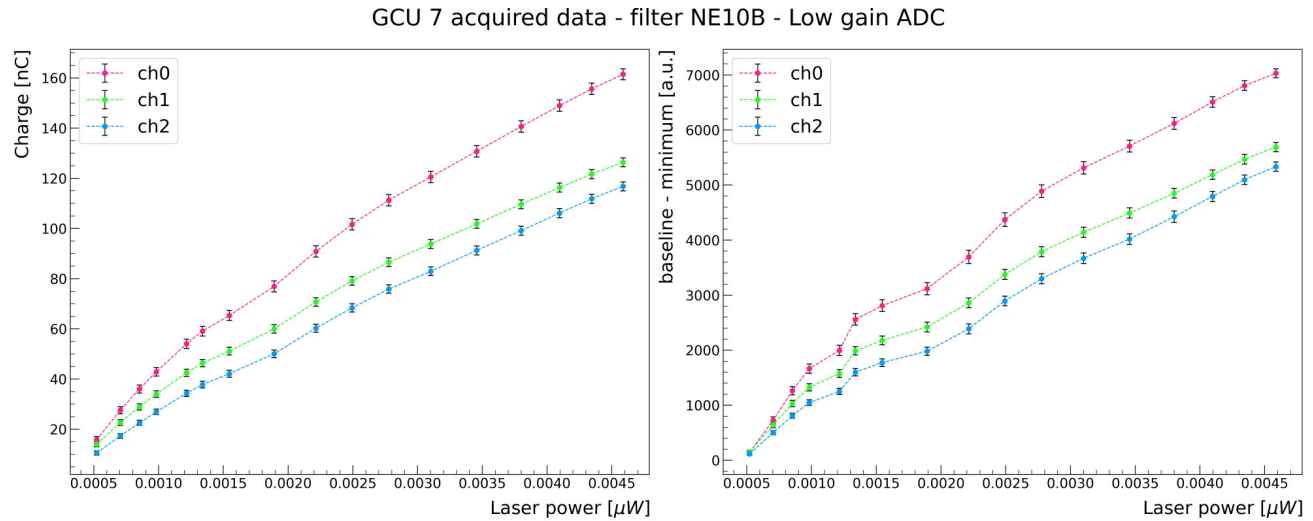


Figure 3.9 – Example of acquired data (GCU7): collected charge (on the left) and signal amplitude (on the right) in function of laser emitted power.

3.2.3 Comparison between LG and HG

In this section data acquired with the two different ADCs are compared in a limited power range (i.e. 6 to 9.6 a.u. in steps of 0.2). Moreover, within this context, the connections GCU - PMT were swapped: GCU12 was originally connected to a PMT located in the higher ring of the cylindrical vessel, whereas GCU7 processed the signals produced by a PMT located in the central ring. This procedure was carried out so as to determine whether or not the energy deposited in the PMTs depends on their positions with respect to the photon source. Comparing **Figure 3.11** and **Figure 3.10**, where the mean collected charge is plotted in function of laser power, with particular attention to data acquired using the HG ADC, we notice that the collected charge shows a significant dependence on the PMT to which the GCU is connected: this might be explained assuming that PMTs are not uniformly illuminated during the measurements. This implies that, although a diffuser was installed inside the vessel, the laser light pulse is not isotropically injected into the liquid scintillator, confirming what was anticipated analyzing **Figure 3.8**.

Global results related to the linearity analysis, concerning both ADCs and for all channels, are provided in Appendix A.

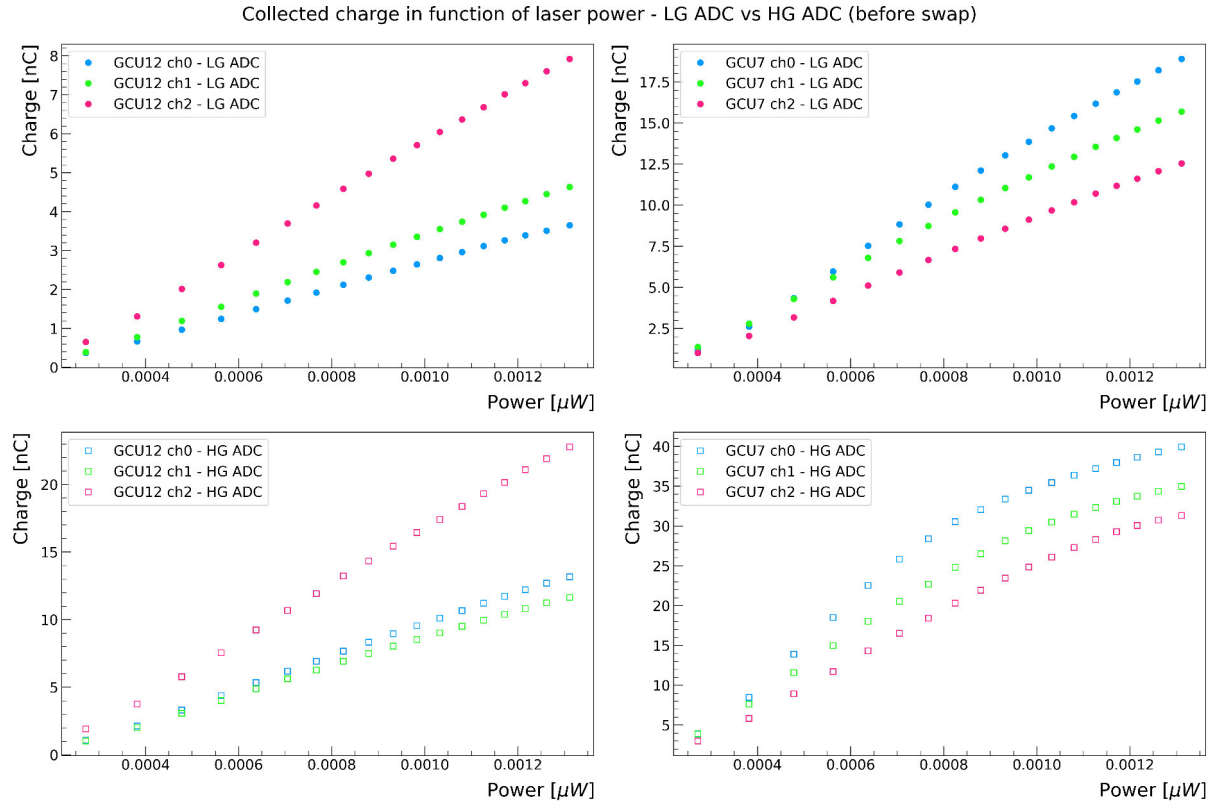


Figure 3.10 – Charge in function of emitted power for two GCUs and both ADCs, before connections swap. GCU12 is connected to a PMT located in the high ring of the vessel, whereas GCU7 to a PMT in the central ring.

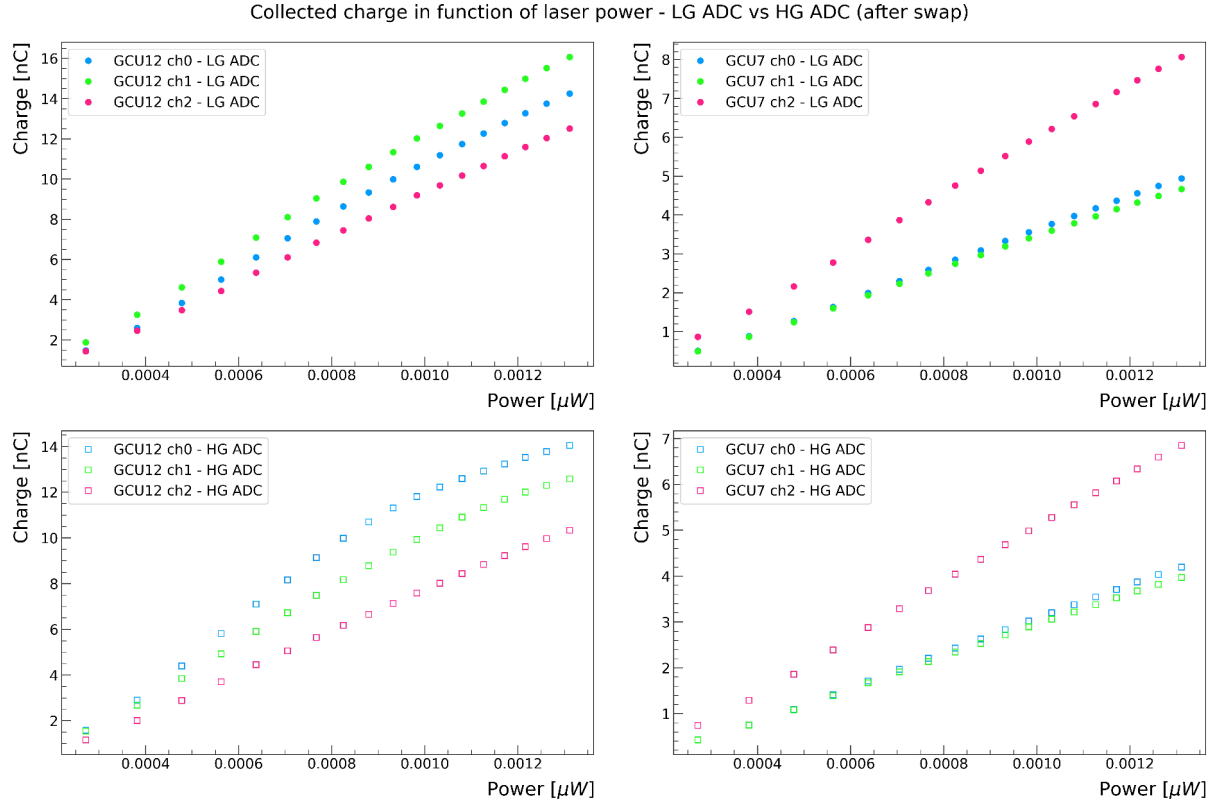


Figure 3.11 – Charge in function of emitted power for two GCUs and both ADCs, after connections swap. GCU12 is connected to a PMT located in the central ring of the vessel, whereas GCU7 to a PMT in the high ring.

Timing analysis

All of JUNO’s GCUs must be synchronized and aligned within a global time in order to correctly timestamp the triggered events. The trigger synchronization accuracy demanded is 16 ns [8]. Since the GCU provides support for the global synchronization process, which is a key feature, a thorough characterization is required. In this section, we will focus our attention on possible trigger jitters between signals related to the same event, i.e. characterized by equal timestamp, evaluating the timing correlation properties between different channels. Additionally, trigger time stability over time will be discussed.

4.1 Trigger and timing system

As previously described in **Section 2.2**, the electronics receives and digitizes the analog signals from the PMTs and transmits the resulting information to the Back End Card (BEC) [5]. The ADU receives the input charge, converts it into a voltage, digitizes the waveform, and sends it to the GCU for further processing. A stream of 14-bit data, sampled at 1 Gsample/s (one sample every 1 ns) is transferred from the ADC to the FPGA, with the data synchronized to a 500 MHz Double Data Rate (DDR) sampling clock. Different GCUs have to be synchronized within 16 ns, as a consequence of the specific operating conditions of the system in use [8]. Moreover, the SERDES (SERializer/DESerializer) introduces a phase uncertainty, resulting in an inherent 8 ns jitter in the trigger time. It follows that signals processed by different GCUs are expected to be synchronized within a time window of 32 ns.

4.2 Study of time correlated signals

With the purpose of studying the timing of the electronics and monitoring data quality, we launched several one-day long runs at a rate of 2 Hz and using the High Gain ADC. First of all, the laser timing was checked by injecting laser pulses into the LS and directly verifying the alignment of the rising edges of signals detected by the single PMTs [11]. Employing an oscilloscope, we evaluated the difference between the signal rising time of a given PMT (the one connected to GCU0 channel 1) and the other PMTs. As can be seen in **Figure 4.1**, the PMTs hit time with respect to a fixed channel was spread out, going from a maximum of 2.4 ± 0.5 ns to a minimum of -1.1 ± 0.2 ns. Nevertheless, the timing of the photons is still sufficiently fast to ensure a feasible procedure to monitor the timing of the electronics.

In order to do so, we defined a fixed timestamp for all the waveforms, specifically the trigger characteristic one t_c , in which the signal reaches an amplitude of 5σ above its baseline. This reference time is calculated during the raw data processing phase and it’s stored in the *trigger time* branch of the ROOT TTree previously described. Once the t_c is retrieved from the TBranch for all the channels, we

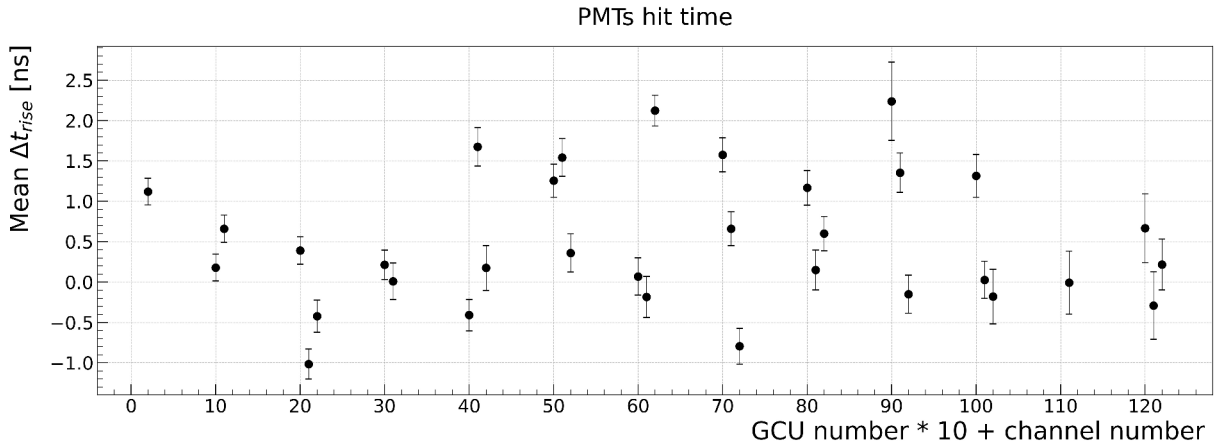


Figure 4.1 – Distribution of PMTs hit time by laser photons in function of channel ID.

evaluated the time differences $\Delta t_c = t_{ic} - t_{0c}$, where t_{ic} is the trigger time of the i-th channel, while t_{0c} is the trigger time of a specific channel that is taken as a reference. In **Figure 4.2**, a reconstructed signal, corresponding to a single event acquired by GCU2 (on the left side by ch0 and ch1, on the right side by ch0 and ch2) is shown: in each plot the time difference Δt_c between the two signals is highlighted in red. An example is depicted on the left plot of **Figure 4.3**, where the differences Δt_c are calculated for GCU2 with respect to channel 0. The majority of Δt_c , for both channels 1 and 2, are within a time interval characterized by a FWHM of $\simeq 1.5 - 2$ ns. The few cases that deviate from this behaviour represent less than 1% of all events. Anyway, both channels are synchronized within a time interval that is well inside the 8 ns requirement.

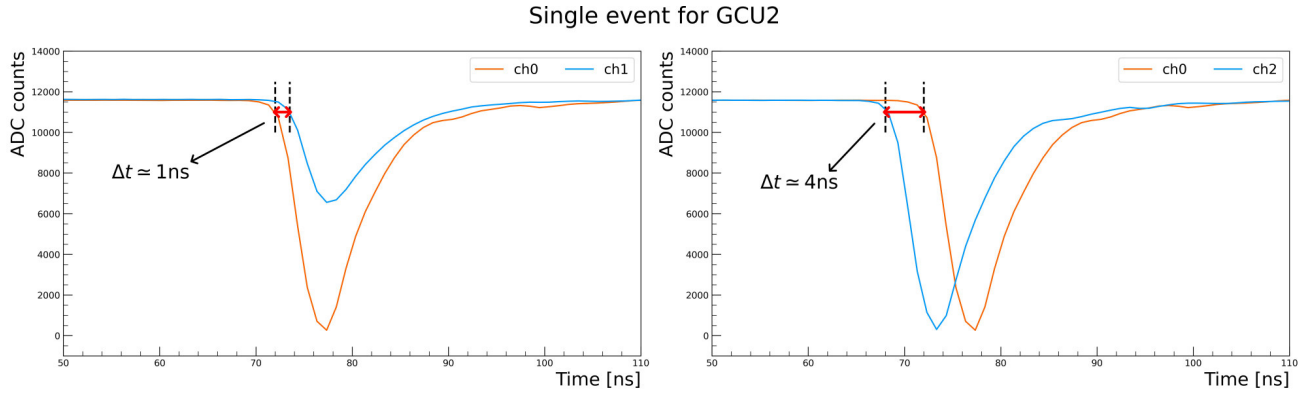


Figure 4.2 – Single event acquired by GCU2: on the left side comparison between ch0 and ch1, on the right side between ch0 and ch2. Time difference between the two signals is highlighted in red.

The same analysis can be conducted evaluating the time differences $\Delta t_c = t_{ic} - t_{0c}$, for all 37 channels: in the specific, the first channel (ch1) of GCU0 is chosen as reference. Global results are reported in Appendix B, whereas an example, for GCU2, is shown on the right panel of **Figure 4.3**. Considering the results, we notice that every channel has its own characteristic time difference with respect to the reference one; in particular, considering the case of GCU2 analyzed in **Figure 4.3** (right), the signals happen to be always before the one acquired by the reference channel.

Furthermore, the mean values retrieved from the histograms in Appendix B are plotted against the channel ID (see **Figure 4.4**). GCU3 ch2 produced a very small signal, due to the undesired presence of ringing and reflection effects. Hence, the information provided by the corresponding PMT is not considered. The majority of the signals deviate in time from the reference trigger time by 26 ns top,

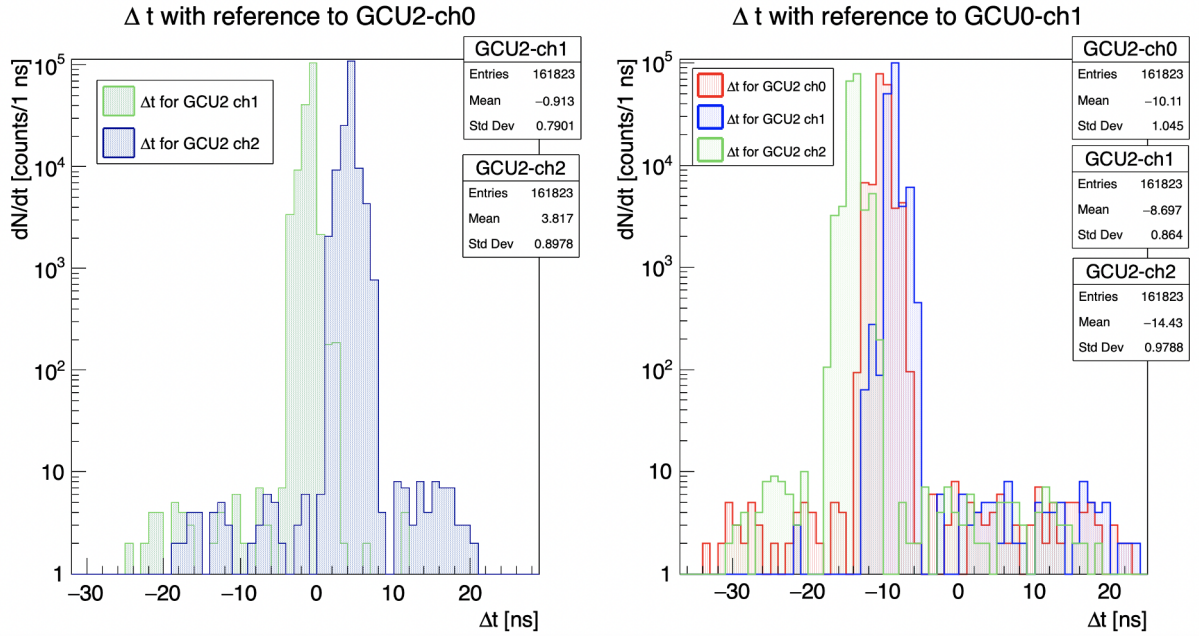


Figure 4.3 – Trigger time delta distribution for GCU2: on the left Δt_c is calculated for channels 1 and 2 with respect to channel 0. On the right, taking as reference GCU0 channel 1.

which is still less than the maximum difference of 32 ns expected in the response of the DAQ system. More substantial deviations may be due to the fact that delays introduced during the PMT photon collection are not taken into account in Δt_c evaluation process. However, it was preliminarily verified (**Figure 4.1**) that this effect does not make a significant contribution. Moreover, comparing data points that concern a fixed GCU (in **Figure 4.4**) we can infer that time correlated signals happen to be synchronized within a maximum of 8-9 ns.

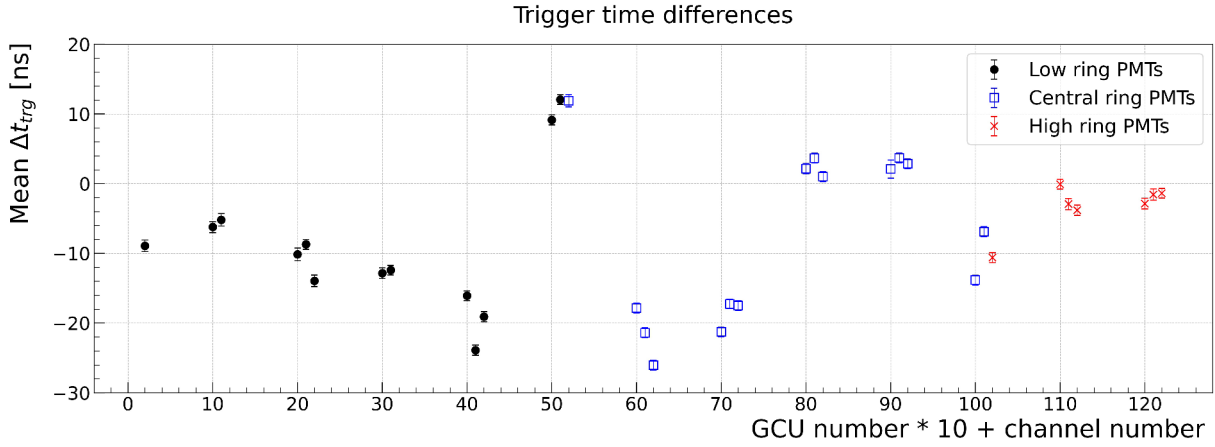


Figure 4.4 – Trigger time differences distribution for all GCUs with reference to GCU0 channel 1. The mean values extracted from the histograms in Appendix B are plotted in function of channel ID. Data points are divided according to the PMTs position inside the vessel.

4.3 Trigger time stability

A more detailed study of time correlated signals has been pursued by evaluating the differences $\Delta t_c = t_{ic} - t_{oc}$ over time; the estimated values are grouped within time intervals of 2 minutes and for each of these groups a histogram, like the ones previously shown, is produced. With the purpose of

studying the behaviour during the 1 day-long data acquisition, the centroids and standard deviations of the histograms are extracted and plotted in function of time.

A preliminary analysis shows that all channels present a similar trend over time, so, as an example, only one plot is reported in **Figure 4.5**. The differences $\Delta t_c = t_{ic} - t_{0c}$, where in this case channels 1 and 2 of GCU2 are considered, happen to be stable during the whole acquisition period. This experimental outcome shows a good agreement with the predictions, thereby playing a key role in the evaluation of the system's reliability.

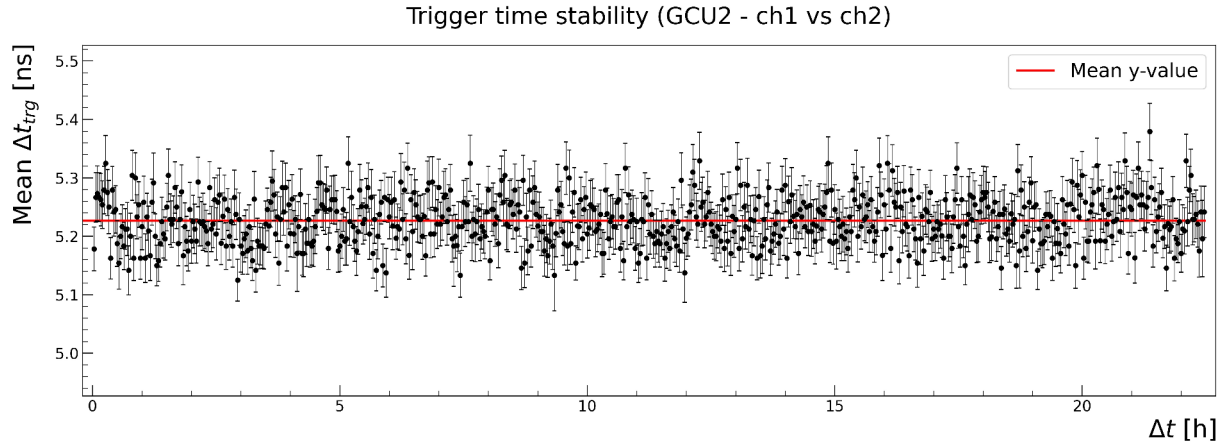


Figure 4.5 – Trigger time delta stability during the whole acquisition between ch1 and ch2 of GCU2.

Measurements with large PMT

In this chapter, a precise characterization of the electronics is pursued following a similar procedure to the one described in **Chapter 3**, but using a different experimental setup; indeed, in this case, the electronics receives and digitizes the analog signals from one large PMT.

5.1 Experimental setup

The signal source is a 20-inch North Night Vision Technologies (NNVT) MicroChannelPlate (MCP)-PMT (**Figure 5.1**), which is also used in the JUNO experiment, secured inside a dark-box. The MCP consists of a two-dimensional array of channels with a 6-20 μm diameter bundled in parallel and formed into the shape of a thin disk. Each channel acts as an independent electron multiplier. The photoelectrons emitted from the photocathode enter the channels of the MCP and impinge on the inner wall where they are multiplied by means of secondary emission. This process is repeated along the channels, and finally a large number of electrons are collected by the anode as an output signal [12]. The PMT is connected, through a BNC connection, to the High Voltage (HV) unit of the UW box. The light inside the dark-box was provided, through an optical fiber, by the same laser used in the LNL setup. A trigger generated by the laser pulse generated was sent to the GCU and the same connections illustrated in **Figure 3.6** were established.



Figure 5.1 – MCP-PMT

5.1.1 Acquired data

In order to monitor data quality and to test the electronics performance, a 12 hours-long run at a rate of 20 Hz was launched. Signals were reconstructed following the same procedure presented in **Section 3.2**. In **Figure 5.2**, 10 uncorrelated (i.e. which do not correspond to the same timestamp) waveforms are reported: we can notice that signals are not perfectly synchronized. This is due to the fact that each PMT has a typical transit time, which is the amount of time it takes for a photoelectron created at the photocathode to travel through the PMT and be detected after being multiplied as an output pulse from the an-

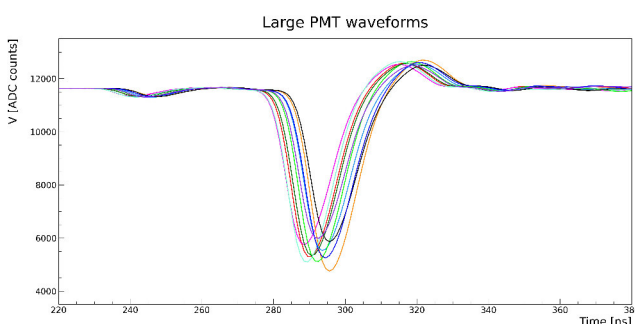


Figure 5.2 – Example of waveforms corresponding to 10 events detected by the large PMT.

ode; this time varies from one photoelectron to the next. Additionally, the visible overshoot is due to an impedance mismatch.

5.2 Linearity analysis

In this section, in order to verify the linearity of the electronics, data from one single GCU channel has been acquired varying laser output power. For this purpose 60 seconds-long acquisitions at 1 kHz were launched. As previously described, information about the charge collected by the single PMTs is retrieved from the specific TBranch, then the centroids and sigmas are extracted and plotted in function of output laser power. In **Figure 5.3** and **Figure 5.4** results obtained using two different filters, NE10B and NE20B respectively, are reported. For the acquisition with the filter that attenuates the beam to 1% of the incident power, a restricted and high laser power range was chosen, so as to guarantee a sufficient amount of light arriving into the PMT. Both plots show excellent linearity right up to saturation conditions, confirming the expected response and performance of the readout electronics.

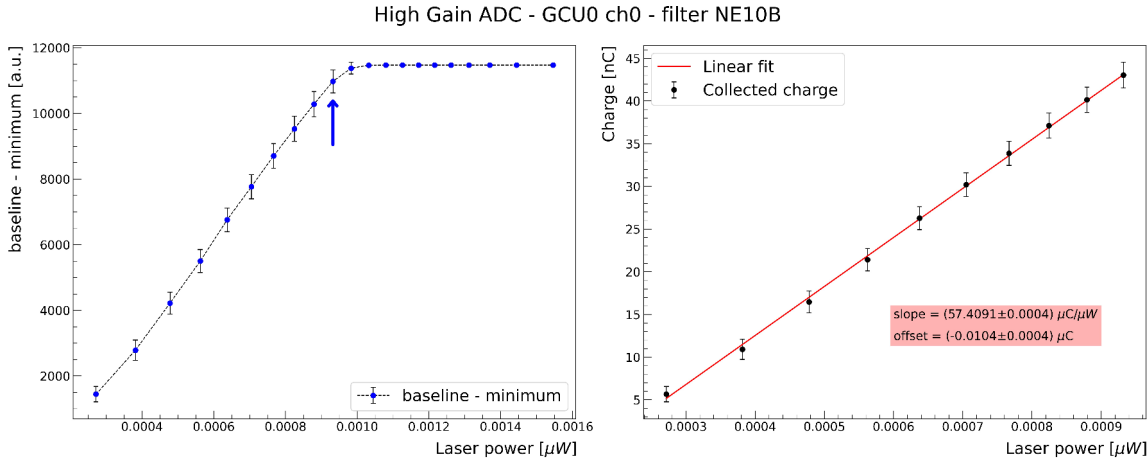


Figure 5.3 – Data acquired with High Gain ADC and filter NE10B: signal amplitude (on the left) and collected charge (on the right) in function of laser emitted power (from 6 to 10 a.u.). The arrow define the linearity range that is consequently considered in the linear regression.

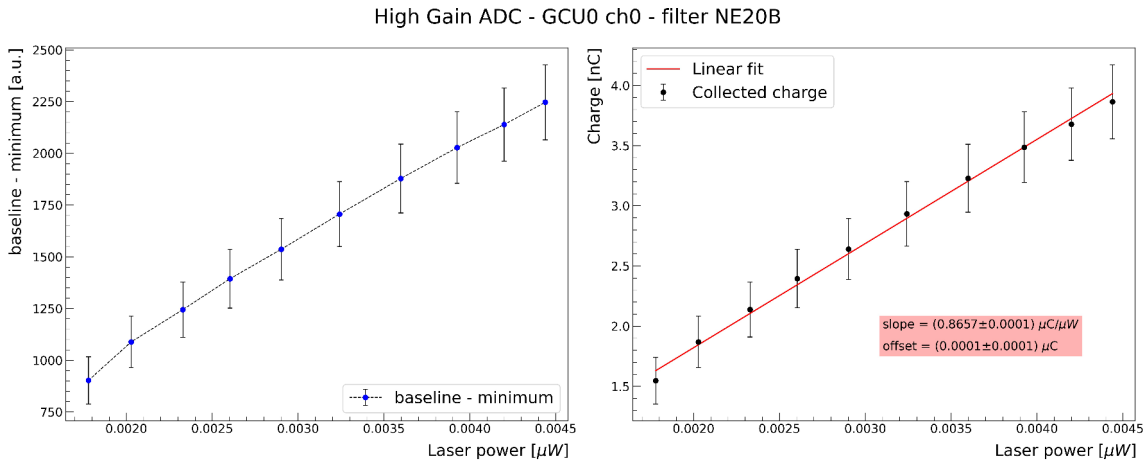


Figure 5.4 – Data acquired with High Gain ADC and filter NE20B: signal amplitude (on the left) and collected charge (on the right) in function of laser emitted power (from 10 to 15 a.u.).

Conclusions and future perspectives

In this thesis, studies on the small PMTs installed on the JUNO test facility at LNL have been performed in order to provide a precise characterization of the electronics: its performance has been investigated in terms of the linearity of the ADC and through time reconstruction. The first feature was studied by employing a laser source characterized by a known wavelength, analyzing the experimental response at different energy inputs. In particular, 60 seconds-long acquisitions were launched varying laser power and using two ADCs with different dynamic ranges. This was possible by means of a charge reconstruction procedure from waveform signals. The linearity of the High Gain ADC was well verified, whereas data acquired with the Low Gain ADC were not suitable to provide accurate results. The second part of the thesis was aimed at studying the timing properties of the system's electronics, in order to verify JUNO synchronization requirements. Time correlated signals turned out to be inside the time window established by the specific operating conditions of the system in use. Generally speaking, the tests confirm the reliability and the expected performance of the whole setup. Additionally, a characterization of the electronics was pursued following similar procedures but using an experimental setup with one large PMT. The linearity response of the ADC was proved, showing an adequate agreement with the expectations. In this case, future and more thorough studies may be foreseen.

For further improvements, the usage of the two ADU amplifiers could be optimized: currently, the incoming analog signals are digitized by both ADCs but data from only one of them is sent to the FPGA and then to the DAQ. An additional feature that allows to read data from both ADCs could be implemented: in this way it would be possible to switch between the two dynamic ranges according to the amplitude of the incoming signal. For example, the saturation level of the HG ADC could be taken as a threshold: if the amplitude is below this level the HG ADC will be used, in order to improve the signal-to-noise ratio; when it's above this limit the LG ADC will be used to provide the output digitized signal.

Appendices

In the following sections detailed plots for all channels of the LNL setup are reported. In particular, **Figure A.1**, **Figure A.2** and **Figure A.3** concern linearity measurements, whereas in **Figure B.1**, **Figure B.2** and **Figure B.3** timing analysis results are shown.

A Detailed results of laser linearity measurements

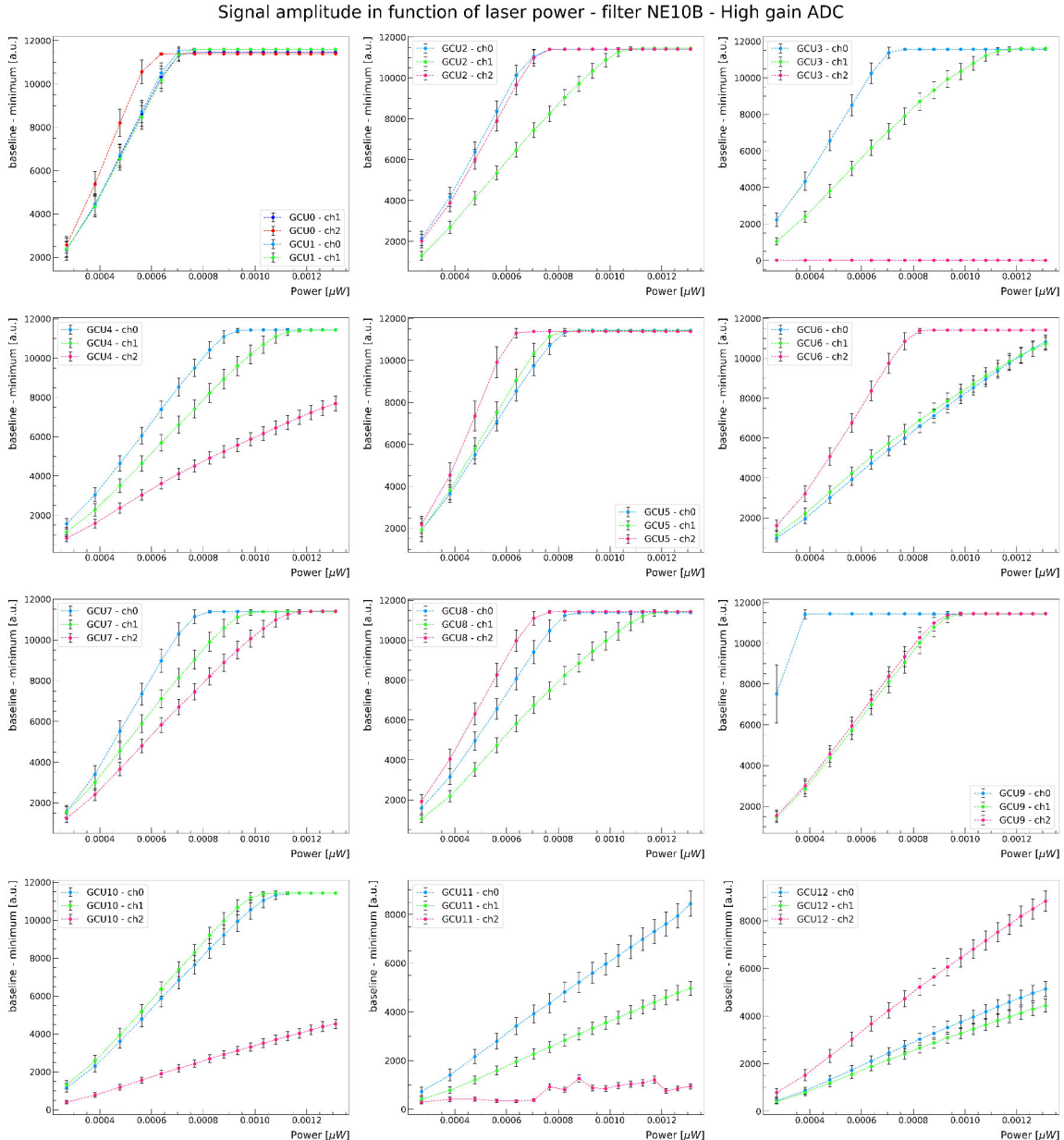
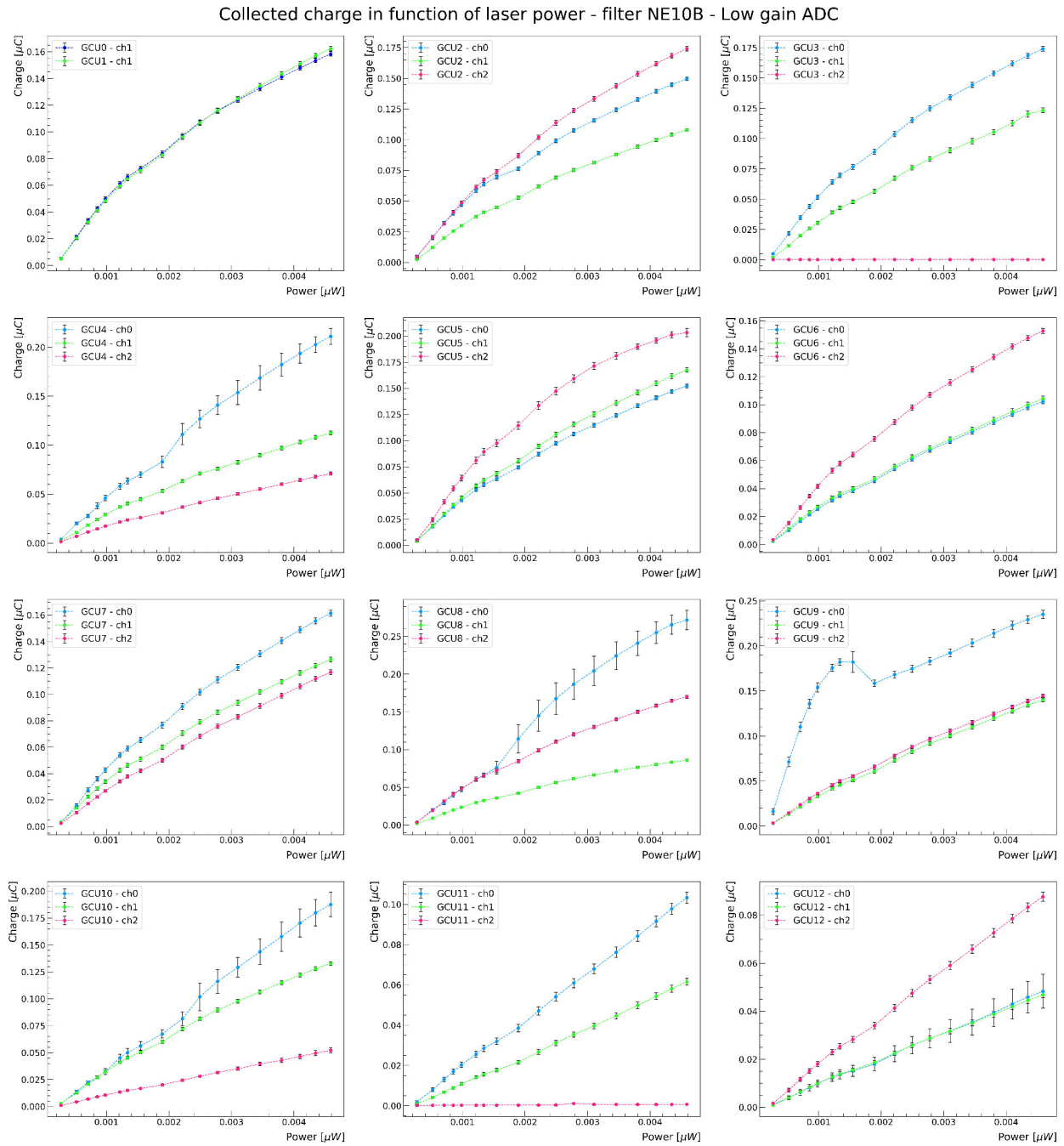
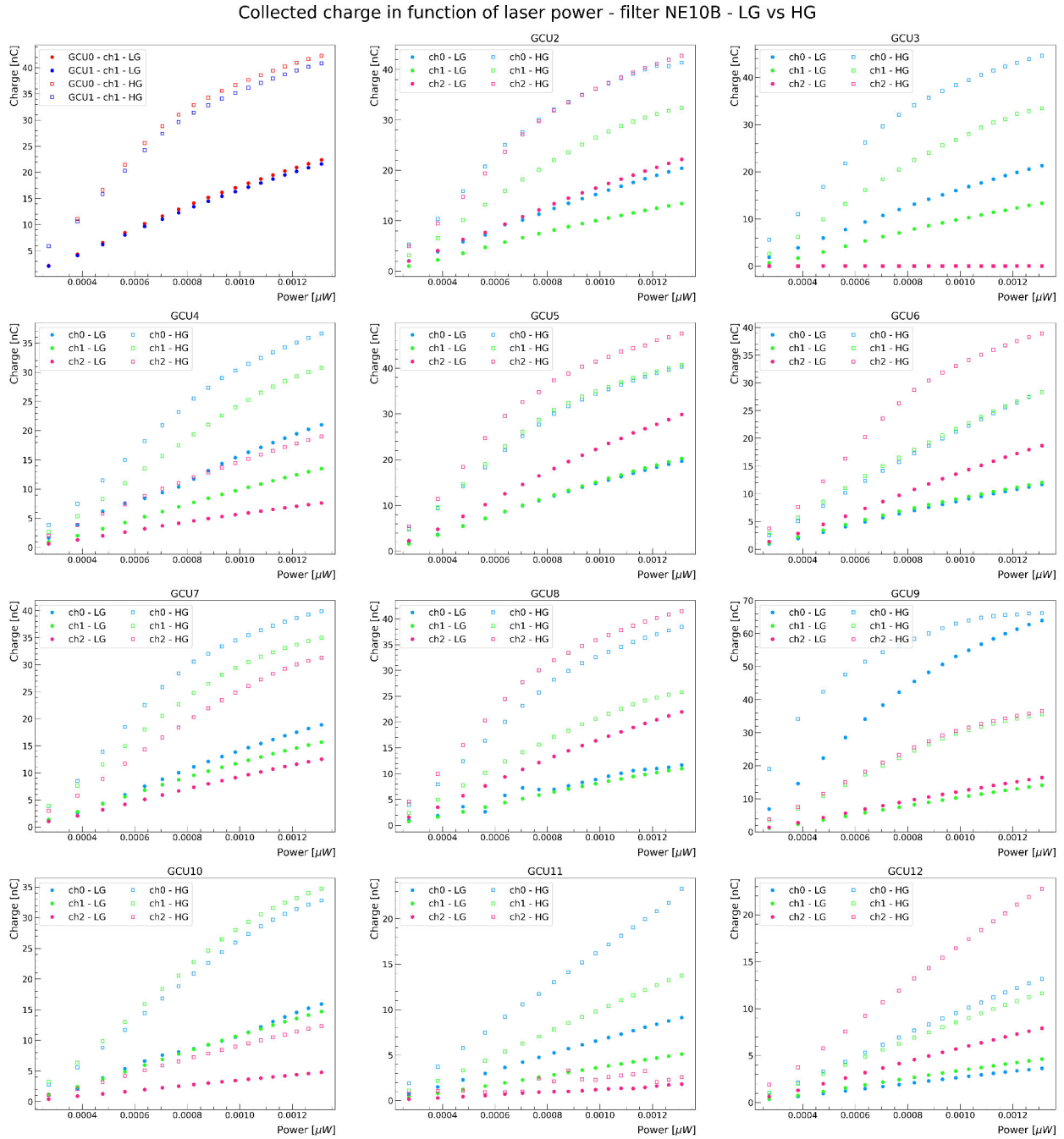


Figure A.1 – Signal amplitude in function of emitted laser power for all channels.
(High Gain ADC - power from 6.0 to 9.6 a.u.)



**Figure A.2 – Charge distribution in function of emitted laser power for all channels.
(Low Gain ADC - power from 6.0 to 15 a.u.)**



**Figure A.3 – Charge distribution in function of emitted laser power for all channels.
(Both ADCs - Power from 6.0 to 9.6 a.u.)**

B Detailed results of timing analysis

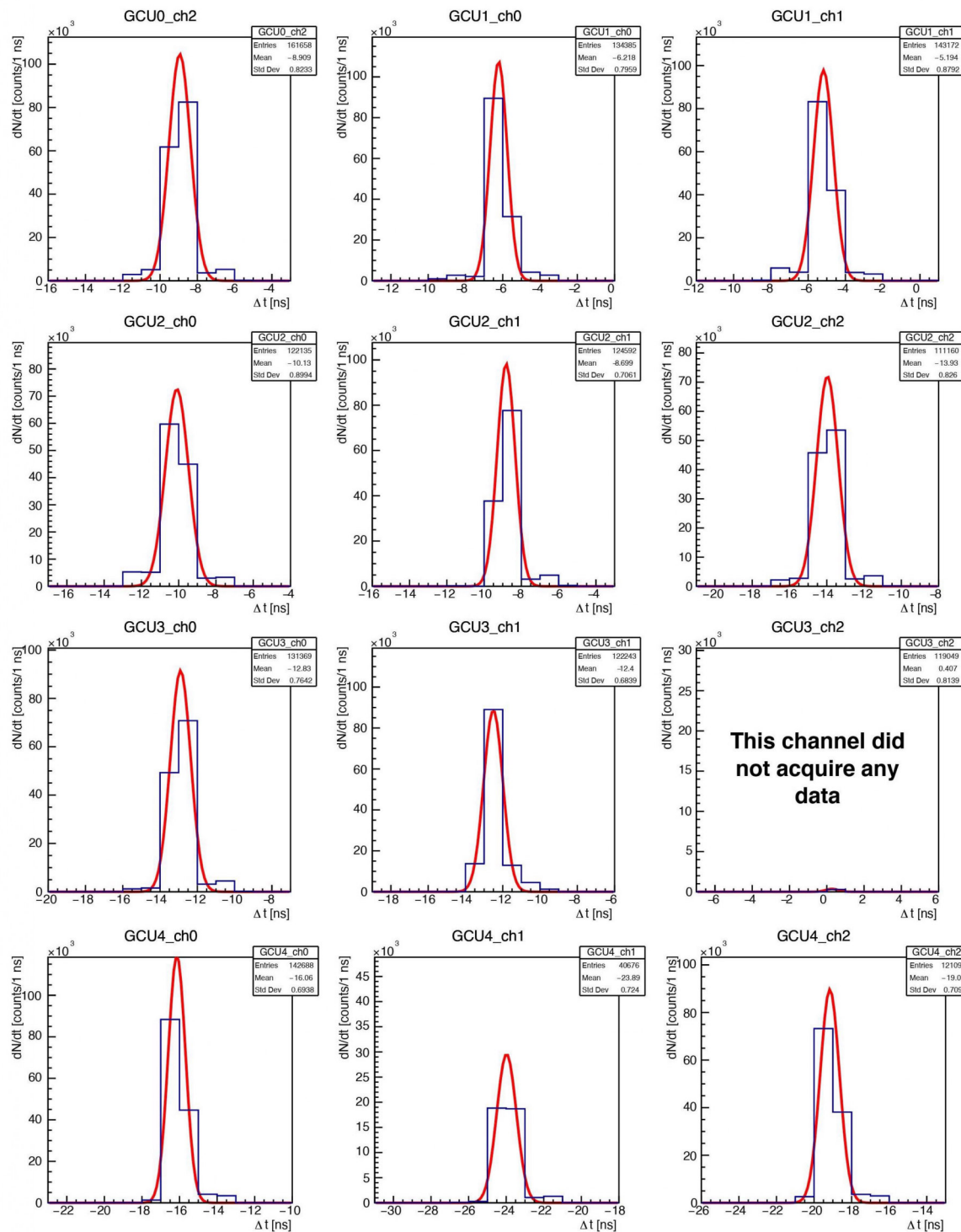


Figure B.1 – Trigger time differences for all channels with reference to GCU0 channel 1 (1).

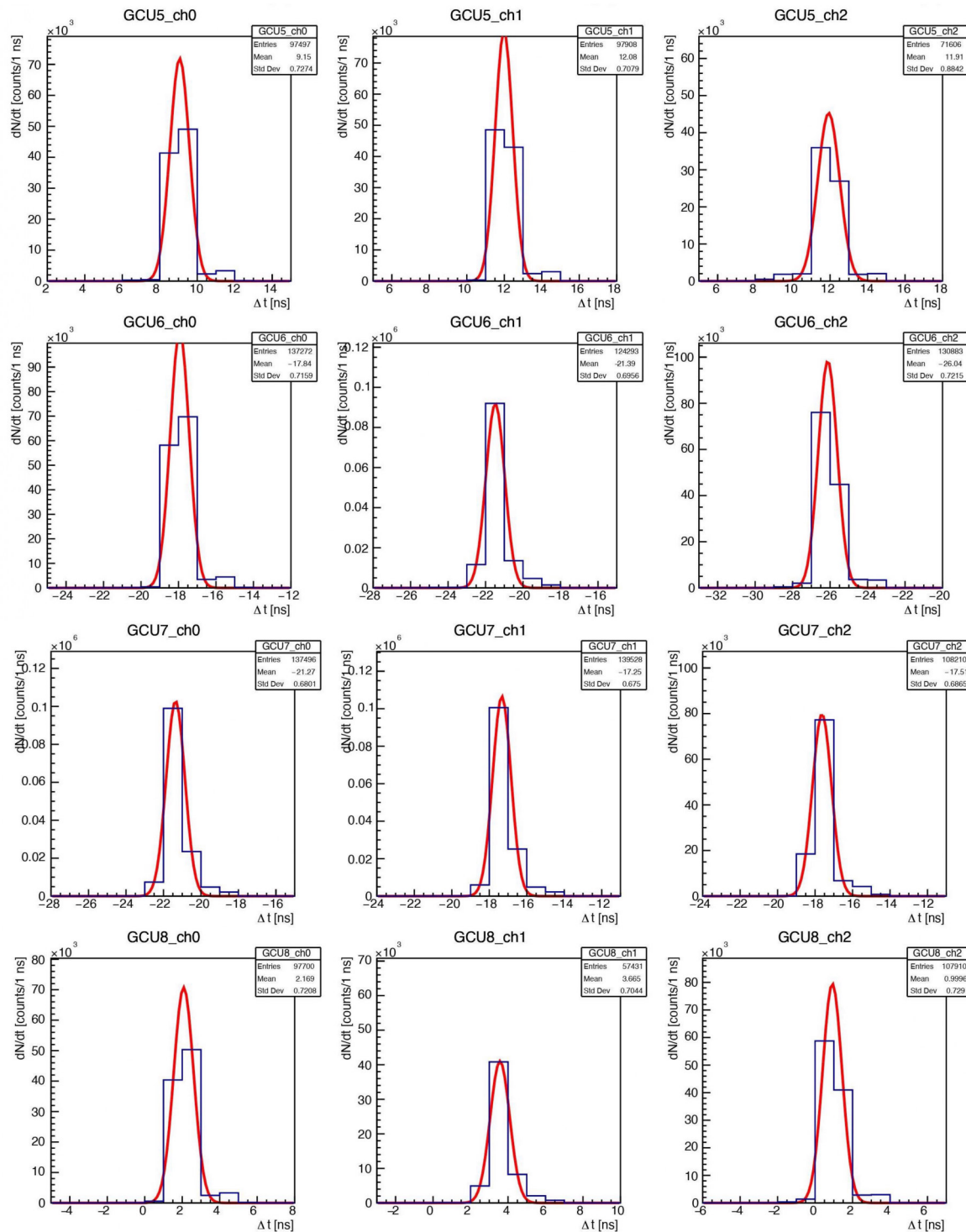


Figure B.2 – Trigger time differences for all channels with reference to GCU0 channel 1 (2).

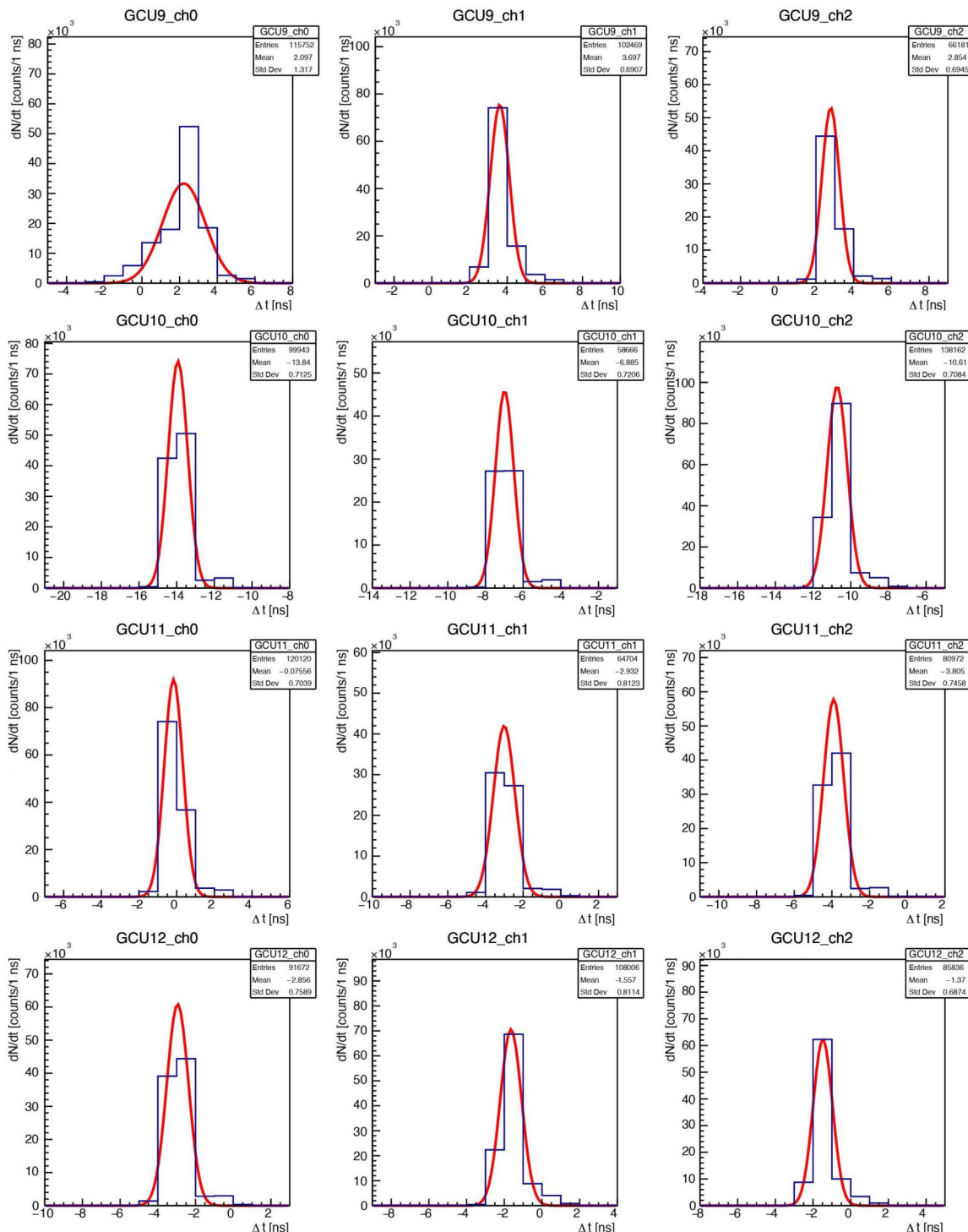


Figure B.3 – Trigger time differences for all channels with reference to GCU0 channel 1 (3).

References

- [1] Z. Djurcic et al., “JUNO Conceptual Design Report” (2015), arXiv: 1508.07166.
- [2] F. An et al., “Neutrino physics with JUNO”, *Journal of Physics G: Nuclear and Particle Physics* 43.3 (2016), p. 030401, arXiv: 1507.05613.
- [3] A. Abusleme et al., “JUNO Physics and Detector”, *accepted by Progress in Particle and Nuclear Physics* (2021), arXiv: 2104.02565.
- [4] A. Abusleme et al., *TAO Conceptual Design Report: A Precision Measurement of the Reactor Antineutrino Spectrum with Sub-percent Energy Resolution*, 2020, arXiv: 2005.08745.
- [5] M. Bellato et al., “Embedded Readout Electronics R&D for the Large PMTs in the JUNO Experiment”, *Nucl. Instr. Meth. A* 985 (2021), p. 164600, arXiv: 2003.08339.
- [6] A. Abusleme et al., “Optimization of the JUNO liquid scintillator composition using a Daya Bay antineutrino detector”, *Nucl. Instr. Meth. A* 988 (2021), p. 164823, arXiv: 2007.00314.
- [7] XP2020 photomultiplier tube, Datasheet, URL: https://wwwusers.ts.infn.it/~rui/univ/Acquisizione_Dati/Manuals/Philips%20XP2020.pdf.
- [8] D. Pedretti et al., “Nanoseconds Timing System Based on IEEE 1588 FPGA Implementation”, *IEEE Transactions on Nuclear Science* 66.7 (2019), pp. 1151–1158, doi: 10.1109/TNS.2019.2906045.
- [9] PLP-10 laser diode head series, Datasheet, URL: https://www.hamamatsu.com/resources/pdf/sys/SOCS0003E_PLP-10.pdf.
- [10] PM16 USB Power Meter, Datasheet, URL: https://www.thorlabs.com/_sd.cfm?fileName=MTN004953-S01.pdf&partNumber=PM16-140.
- [11] Y. Zhang et al., “Laser calibration system in JUNO”, *Journal of Instrumentation* 14.01 (2019), p. 01009, arXiv: 1811.00354v4.
- [12] Hamamatsu Photonics K.K., *PHOTOMULTIPLIER TUBES, Basics and Applications*, 2007.
- [13] F. Marini, *Design and tests of the FPGA embedded trigger algorithms for the large PMT JUNO Electronics*, A.A. 2017/2018, Master Degree in Physics.
- [14] R. Callegari, *Characterization and tests of 39 channels of the JUNO large PMT electronics*, A.A. 2019/2020, Master Degree in Physics.
- [15] E. Tuzza, *Studio della risposta temporale di fotomoltiplicatori di grandi dimensioni per esperimenti sulla fisica del neutrino*, A.A. 2015/2016, Laurea in Fisica.